

Supplementary Information for

First-principles study of superionic $\text{Na}_{9+x}\text{Sn}_x\text{M}_{3-x}\text{S}_{12}$ (M = P, Sb)

Anastassia Sorokin^a and Stefan Adams^{*a}

1. Details of the Computational methods

All DFT-based first-principles calculations were performed by the Vienna *Ab initio* Simulation Package (VASP 5.3.3) [1, 2]. The ion-electron interaction was depicted by the projector augmented wave (PAW) method [3], and the exchange-correlation (X-C) was described by two functionals: the generalized gradient approximation (GGA) developed by Perdew, Burke, and Ernzerhof (PBE) [4], and the improved GGA-PBE for densely packed solids and their surfaces (PBEsol) [5].

During VASP calculations we used PAW potentials implemented in VASP: $3s^12p^6$ electrons were treated as valence electrons for Na (Na_pv 19Sep2006), $3s^23p^3$ for P (P 6Sep2000), $5s^25p^3$ for Sb (Sb 6Sep2000), $3s^23p^4$ for S (S 6Sep2000), and $4d^{10}5s^25p^2$ for Sn (Sn_d 06Sep2000). The energy convergence criterion for electronic self-consistency was at least 10^{-5} eV per atom and the plane wave cutoff energy of 520 eV was employed. The k -points meshes were (999) for Na_3PS_4 with 16 atoms in the supercell, (778) for Na_4SnS_4 with 18 atoms, (555) for $\text{Na}_{10}\text{SnP}_2\text{S}_{12}$ and $\text{Na}_{10}\text{SnSb}_2\text{S}_{12}$ with 50 atoms and (222) for the $\text{Na}_{12-x}\text{Sn}_{3-x}\text{P}_x\text{S}_{12}$ and $\text{Na}_{12-x}\text{Sn}_{3-x}\text{Sb}_x\text{S}_{12}$ at $0.625 \leq x \leq 1.375$ with 205-211 atoms. To gain accurate total energy, the calculations were performed by the tetrahedron method incorporating a Blöchl correction [6]. Visualization employed the VESTA software (Visualization for Electronic and Structural Analysis) [7]

Ab initio molecular dynamics (AIMD) simulations were performed using the VASP code in terms of a canonical ensemble (NVT) with a Nosé thermostat [8,9] at 300, 600, 800, 1000, 1200 and 1400 K. The Newton's equation of motion was solved via the Verlet algorithm [10] with a time step of 2 fs for 300, 600 and 800 K and 1 fs at 1000, 1200 and 1400 K., and a total simulation time of ~80 ps. The AIMD simulations were performed on the $(1 \times 1 \times 1)$ Γ -point with energy cutoff of 360 eV and the X-C functional of PS. The coefficient of diffusion was determined at each temperature from a linear fitting as

$$D = \frac{1}{2dt} \langle [\Delta r(t)]^2 \rangle \quad (\text{S1})$$

where d is the dimension of diffusion, t is time, and $\langle [\Delta r(t)]^2 \rangle$ is the mean square displacement of sodium ions. Then activation energy E_a was found by fitting the Arrhenius equation,

$$D = D_0 \exp\left(\frac{-E_a}{k_B T}\right) \quad (\text{S2})$$

where D_0 is the pre-exponential factor, k_B is Boltzmann's constant, and T is temperature. The sodium ionic conductivity σ was derived from the generalized Nernst-Einstein equation:

$$\sigma(T) = \frac{cz^2F^2}{H_R RT} D(T) \quad (\text{S3})$$

where c , z , F , and R are the molar density of sodium ions, the charge of a sodium ion, Faraday constant and gas constant respectively. The Haven ratio $H_R \approx 0.5$ takes into account a moderate degree of correlation between successive hops. For the few fast-ion conductors, where reliable H_R values are available, some degree of correlation is practically always noted (with typical Haven ratio values of $0.3 \leq H_R \leq 0.75$), so that $H_R \approx 0.5$ should be a more useful approximation than the common simplification $H_R=1$ (i.e. no correlation).

To identify the distribution of Na site occupancy (i.e. number of Na in the simulated unit cell divided by Wyckoff site multiplicity) and monitor the hops among the partially occupied Na sites, all frames from the ab-initio models of $\text{Na}_{88}\text{Sn}_{16}\text{M}_8\text{S}_{96}$ (M=P, Sb) were subdivided into a rectangular $4 \times 4 \times 8$ grid. As there was no significant drift of the model, this grid was kept fixed over the runtime of the AIMD simulation. Of the resulting 128 volume elements 16 are occupied by the SnS_4 tetrahedra, 8 by the MS_4 tetrahedra

(M=P, Sb) and the remaining 104 volume elements are available for the Na. These 104 sites practically coincide with the Voronoi polyhedra of the 16f (Na1), 32g (Na2), 16d (Na3), 16c (Na4), 16e (Na5) and 8b (Na6) sites. A self-written analysis software tracked the motion of each Na in each time step to identify the frequency of hops.

Correlations between the motion of Na and S atoms within the AIMD simulations are analysed with the help of the van Hove correlation functions. The Van Hove function $G(r,t)$ is the probability density of finding a particle i in the vicinity of r at time t , knowing that a particle j has been at the origin at time $t=0$. The self- and distinct parts of the van Hove function are analysed separately, as they have distinct physical meanings. The self part $G_s(r,t)$ represents the probability density of finding the same particle that was at the origin at time $t = 0$ at the distance r after a time interval t (i.e. the case $i = j$), while the distinct part $G_d(r,t)$ represents the probability density of finding a different particle j ($j \neq i$) at the distance r a time interval t after particle i had been at the origin.

The modelling of pathways for mobile Na^+ as regions of low bond valence site energy, $E_{BVSE}(\text{Na})$, has been demonstrated to be a simple and reliable way of identifying transport pathways in local structure models, provided that the local structure model captures the essential features of the real structure. The bond length $R_{\text{Na-S}}$ between a Na^+ cation and an anion S^{2-} can with the help of tabulated empirical parameters $R_{0,\text{Na-S}}$ and $b_{\text{Na-S}}$ to an individual bond valence $s_{\text{Na-S}}$ (as seen in Eq. S4),

$$s_{\text{Na-S}} = \exp[(R_{0,\text{Na-S}} - R_{\text{Na-S}}) / b_{\text{Na-S}}] \quad (\text{S4})$$

Both $s_{\text{Na-S}}$ and the bond valence sum mismatch $|\Delta V(\text{Na})|$, i.e. the deviation of the observed sum of all bond valences around a central Na^+ from the expectation value (the formal valence of the ion), are conventionally expressed in arbitrary “valence units”. As elaborated by our group,[12,13,14] they can, however, be linked to an absolute energy scale by expressing the bond valence as a Morse-type interaction energy between cation Na^+ and anion S^{2-} as shown in Eq. S5, which brings the bond valence-related Morse term and the Coulomb repulsion $E_{repulsion}$ term on the same scale.

$$E_{BVSE}(\text{Na}) = \sum_x D_0 \left[\sum_{i=1}^N \left(\left(\frac{s_{\text{Na-S}}}{s_{\text{min,Na-S}}} \right)^2 - \frac{2 \cdot s_{\text{Na-S}}}{s_{\text{min,Na-S}}} \right) \right] + E_{repulsion} \quad (\text{S5})$$

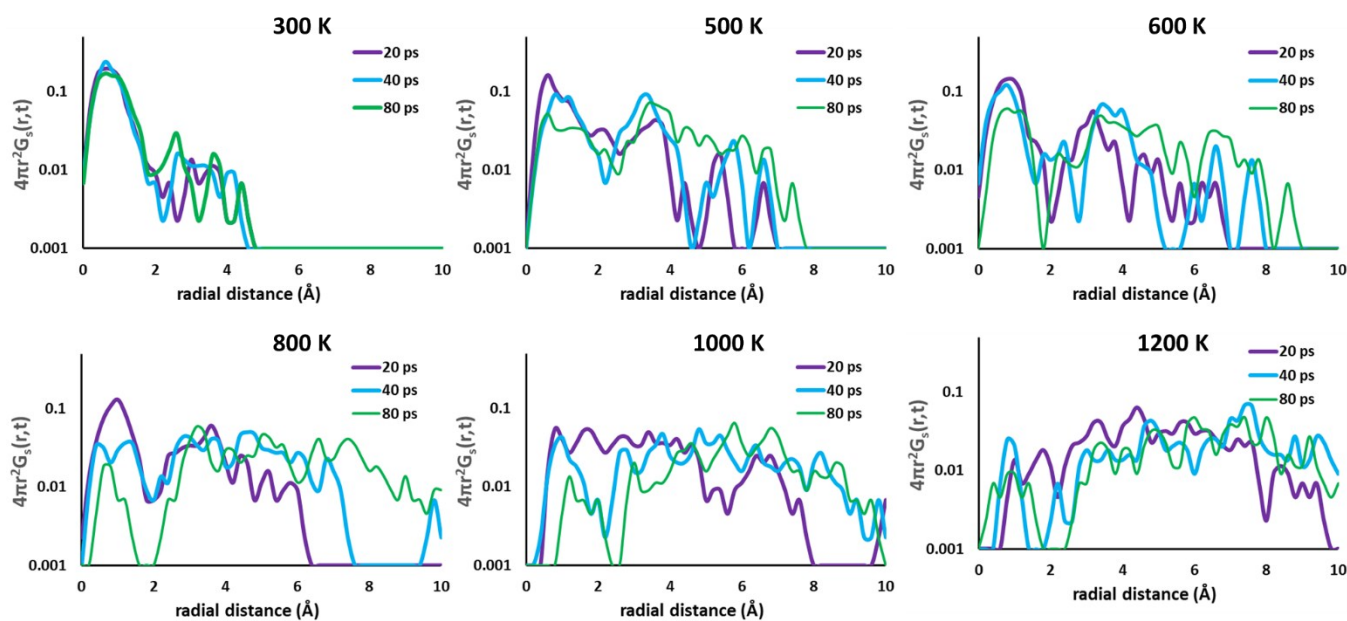
The required bond valence parameters R_0 and b are taken from our *softBV* database as published in ref. [15]. Migration pathways for Li^+ are analyzed as regions of low bond valence site energy $E_{BVSE}(\text{Na})$ in grids spanning the structure model with a resolution of *ca.* $(0.1\text{-}0.2 \text{ \AA})^3$. Starting from an analysis of local minima and saddle points of $E_{BVSE}(\text{Na})$, the grid analysis utilizes a modified Dewar, Healy and Stewart (DHS)-related path finding algorithm to identify low energy paths connecting the local site energy minima. For the purpose of analyzing $E_{BVSE}(\text{A})$ landscapes, Coulomb repulsions are considered only between mobile and immobile cations. Coulomb attraction terms are generally integrated into the Morse attraction term. The charge screening is based on an error function complement term $E_{repulsion}$ as indicated in equation S6,

$$E_{repulsion}(A-B) = \frac{q_A q_B}{R_{A-B}} \cdot \text{erfc} \left(\frac{R_{A-B}}{f \cdot (r_A + r_B)} \right) \quad (\text{S6})$$

where r_A , r_B are the covalent radii of the respective cation (or anion) pair A , B and f is a screening factor (typically of the order $f \approx 0.75$) that is empirically linked to the electronegativity distribution in the respective crystal structure. In practice, our software tool varies f for each compound before calculating the pathways to achieve ambient pressure when using the *softBV* forcefield. Both the Morse-type interactions and the Coulomb-repulsion terms are force-shifted to ensure zero energy gradients at the cut-off distance.

Our samples of $\text{Na}_{11}\text{Sn}_2\text{PS}_{12}$ and $\text{Na}_{11}\text{Sn}_2\text{SbS}_{12}$ contained 208 atoms. We built $\text{Na}_{11}\text{Sn}_2\text{PS}_{12}$ and $\text{Na}_{11}\text{Sn}_2\text{SbS}_{12}$ samples possessing $I4_1/acd$ space symmetry containing 208 atoms. The initial sizes of the systems were $13.608 \times 13.608 \times 27.159 \text{ \AA}$ for $\text{Na}_{11}\text{Sn}_2\text{PS}_{12}$ and $13.829 \times 13.829 \times 27.159 \text{ \AA}$ 16 Sn atoms were placed in the 16e Wyckoff sites, 8 P (or Sb) atoms were placed in 8a sites, 96 S atoms were placed in 32g sites in such a way that they formed SnS_4 and PS_4 (SbS_4) tetrahedra that delimit wide Na^+ -ion channels along the c axis and within the ab planes. Na atoms could occupy 88 positions from 16f (Na1), 32g (Na2), 16d (Na3), 16c (Na4), 16e (Na5) and 8b (Na6) as in ref. [8], cf. Table S.1.

Self part of the van Hove correlation function $4 \pi r^2 G_s(r)$ for Na Atoms



Distinct part of the van Hove correlation function $G_d(r)$ for Na Atoms

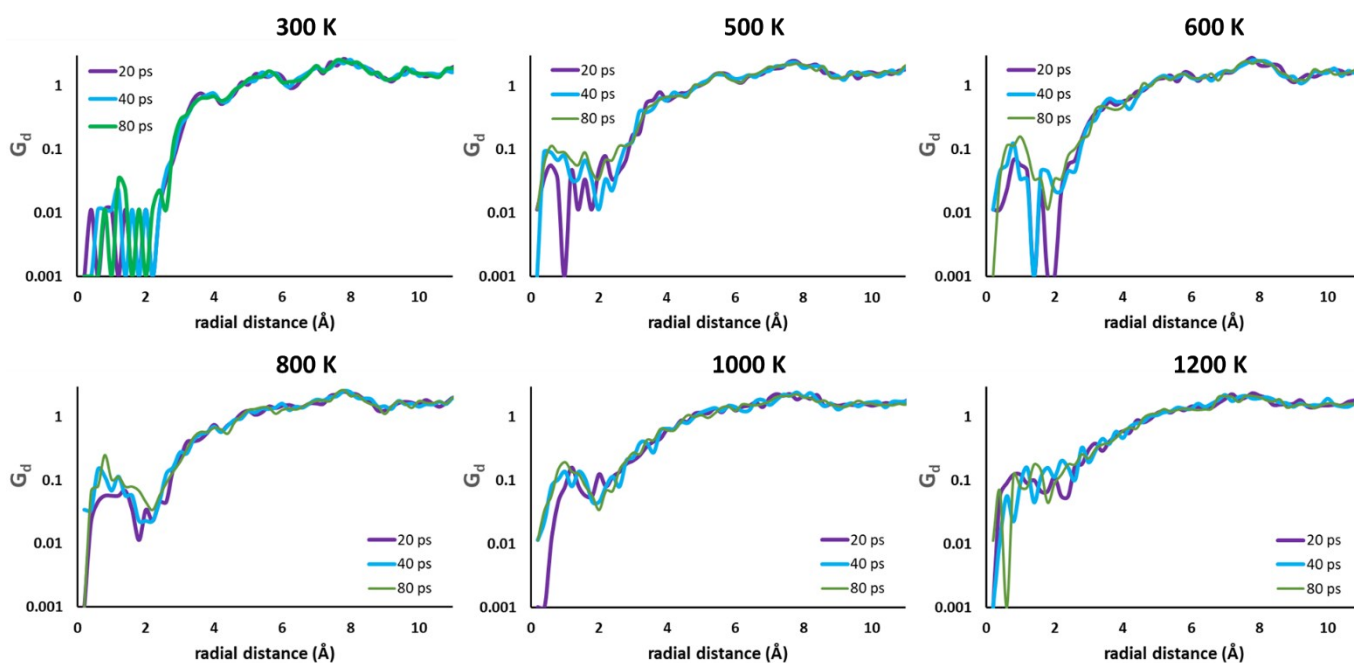
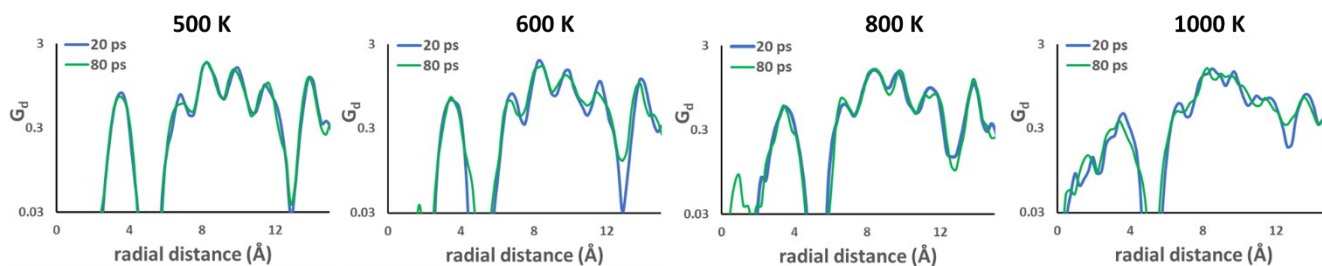


Figure S.1. Semilogarithmic plots of the self part self part $4 \pi r^2 G_s(r)$ (top) and distinct part $G_d(r)$ (bottom) of the van Hove correlation function for the Na atoms in the AIMD simulations of $\text{Na}_3\text{Sn}_2\text{PS}_{12}$ at 300 – 1200 K over 20, 40 or 80 ps as a function of the radial distance r .

Distinct part of the van Hove correlation function $G_d(r)$ for S Atoms in PS_4 groups



Distinct part of the van Hove correlation function $G_d(r)$ for S Atoms in SnS_4 groups

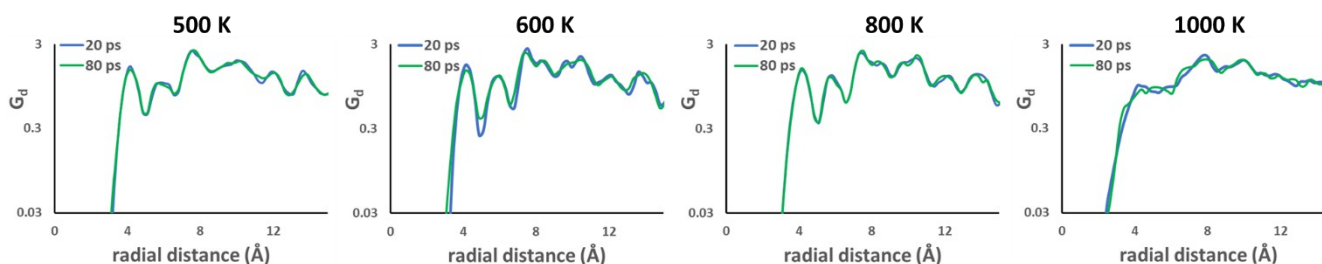


Figure S.2. Semilogarithmic plots of the distinct part $G_d(r)$ of the van Hove correlation function for the S atoms in the AIMD simulations of $Na_{11}Sn_2PS_{12}$ at 500 – 1000 K over 20 or 80 ps as a function of the radial distance r . Graphs in the top row refer to the S atoms within PS_4 groups, where for $T \geq 600$ K a peak at $r < 2$ Å appears. This shows that the original S left the site and a different S can occupy this site by the rotation of the PS_4 groups. Graphs in the bottom row refer to the S atoms within SnS_4 groups. In that case the original S vibrates around the same position, so that no other S can assume this position. Consequently, $G_d(r)$ for $r < 2$ Å remains zero at all displayed temperatures.

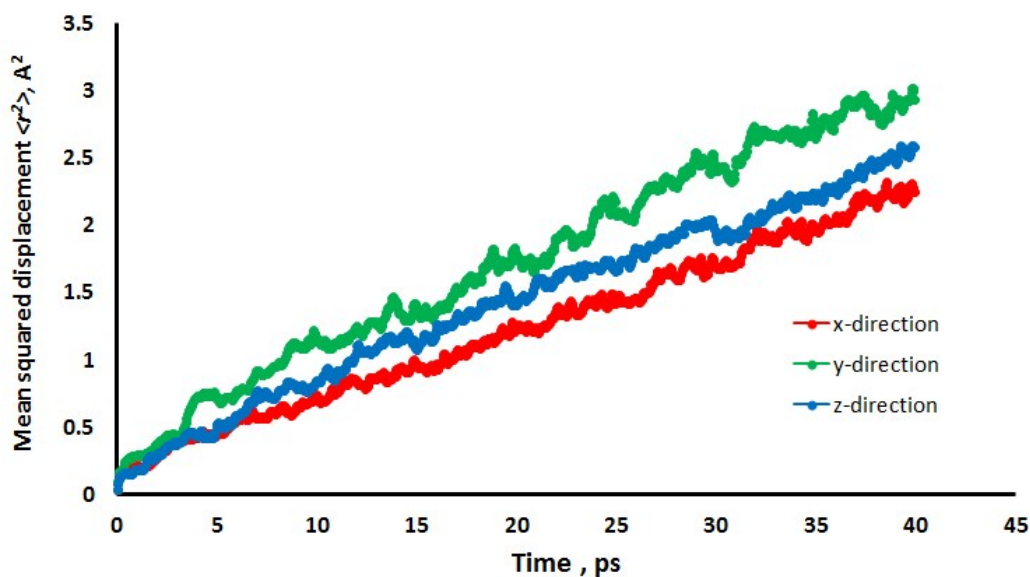


Figure S.3. Mean square displacement of Na ions for long-time simulation of $Na_{11}Sn_2PS_{12}$ at 600 K as function of simulation time in x-, y- and z-directions.

2. Starting structure models

Table S.1 Atomic positions and occupancies for $\text{Na}_{11}\text{Sn}_2\text{PS}_{12}$ (taken from [16]) and $\text{Na}_{11}\text{Sn}_2\text{SbS}_{12}$ (occupancies taken from [17] for $\text{Na}_{11.25}\text{Sn}_{2.25}\text{Sb}_{0.75}\text{S}_{12}$) samples.

Atom	Wyckoff site	Occupancy for $\text{Na}_{11}\text{Sn}_2\text{PS}_{12}$	Occupancy for $\text{Na}_{11.25}\text{Sn}_{2.25}\text{Sb}_{0.75}\text{S}_{12}$	x	y	z
<i>Na1</i>	16 <i>f</i>	0.98	0.97	0.2615	0.0115	-0.1250
<i>Na2</i>	32 <i>g</i>	0.83	0.95	0.0103	-0.0168	-0.1254
<i>Na3</i>	16 <i>d</i>	0.82	0.95	0	0.2500	0.0075
<i>Na4</i>	16 <i>c</i>	0.93	0.83	0	0	0
<i>Na5</i>	16 <i>e</i>	0.95	0.98	0.2500	0.2748	0
<i>Na6</i>	8 <i>b</i>	0.12	0	0	-0.25	-0.1250
<i>P (Sb)</i>	8 <i>a</i>	1	1	0	-0.2500	0.1250
<i>Sn</i>	16 <i>e</i>	0.95	1	0.2500	0.0249	0
<i>S1</i>	32 <i>g</i>	0.95	1	0.0843	-0.1604	0.0817
<i>S2</i>	32 <i>g</i>	1	1	0.1477	0.1244	0.0503
<i>S3</i>	32 <i>g</i>	1	1	0.1512	-0.0765	-0.0513

3. Summary of decomposition energies and volume/atom data

Table S.2. Synopsis of decomposition energies and volume/atom data of tertiary and quaternary compounds $\text{Na}_{9+x}\text{Sn}_x\text{P}_{3-x}\text{S}_{12}$ and $\text{Na}_{9+x}\text{Sn}_x\text{Sb}_{3-x}\text{S}_{12}$ from this work as well as from literature computational or experimental data.

	Method	Decomposition energy (eV/atom) ^{a)}	Volume ($\text{\AA}^3/\text{atom}$)
Na_3PS_4	PBE, this work		21.973
	PBE, (16)		22.019
	PBEsol, this work		20.892
	PBEsol, (16)		20.946
	Expt., (ICSD)		21.373
Na_4SnS_4	PBE, this work		24.477
	PBEsol, this work		21.557
	Expt., (ICSD)		23.714
Na_3SbS_4	PBE, this work		24.018
	PBEsol, this work		22.746
	Expt., (ICSD)		23.038
$\text{Na}_{11}\text{Sn}_2\text{PS}_{12}$	PBE, this work	-3.301	25.048
	PBE, (16)	-1.906	25.056
	PBE, (18)	14.5	25.061
	PBEsol, this work	2.952	23.916
	PBEsol, (16)	2.979	23.508
	Expt. (16)		24.1
	Expt. (19)		24.258
	Expt. (20)		24.178
	PBE, (21)	~3	24.673
	Expt., (22)		24.261
$\text{Na}_{11}\text{Sn}_2\text{PS}_{12}$ (quenched from 1200 K)	PBE, this work	6.51	25.318
$\text{Na}_{10}\text{SnP}_2\text{S}_{12}$	PBE, this work	6.248	25.757
	PBE, (16)	11.312	26.125
	PBE, (18)	18.06	
	PBE, (23)	7.1	25.543
	Expt., (16)	23.677	24.728
$\text{Na}_{11}\text{Sn}_2\text{SbS}_{12}$	PBE, this work	-3.234	26.838
	PBEsol, this work	3.80	24.683
	Expt., (17)		25.3
	Expt., (23)		25.17

^{a)} relative to the corresponding ternary compounds.

4. Effect of phase transition on structure and ion mobility

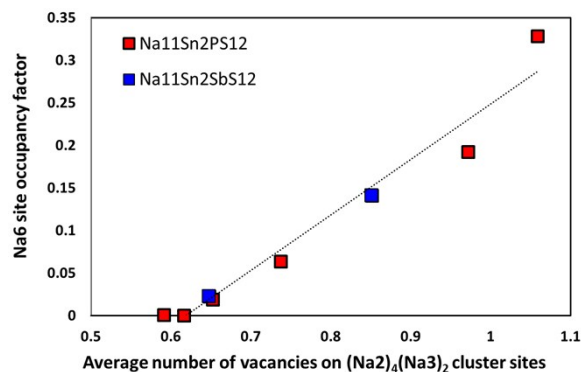


Figure S.4 Correlation between the occupancy of the Na6 site and the vacant sites in the surrounding group in the high temperature phase AIMD simulations of Na₁₁Sn₂PS₁₂ (red squares) and Na₁₁Sn₂SbS₁₂ (red squares). The dotted line represents a linear regression over all data as a guide to the eye.

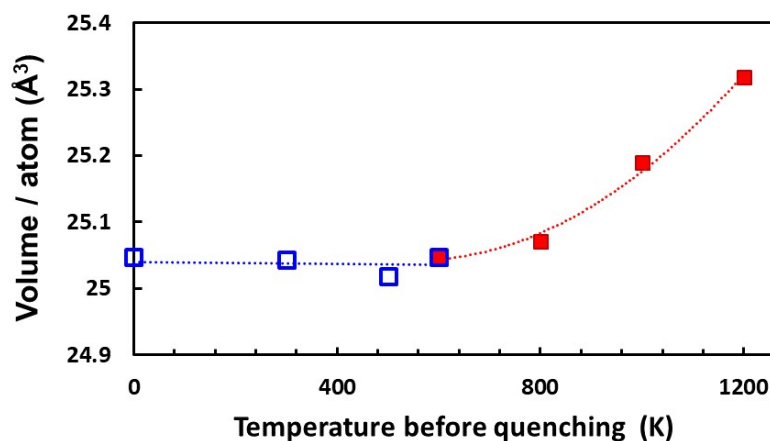


Figure S.5 Correlation between the volume per atom of relaxed structure models “quenched” from the final states of AIMD simulations and the AIMD temperature as a measure for the state of disorder.

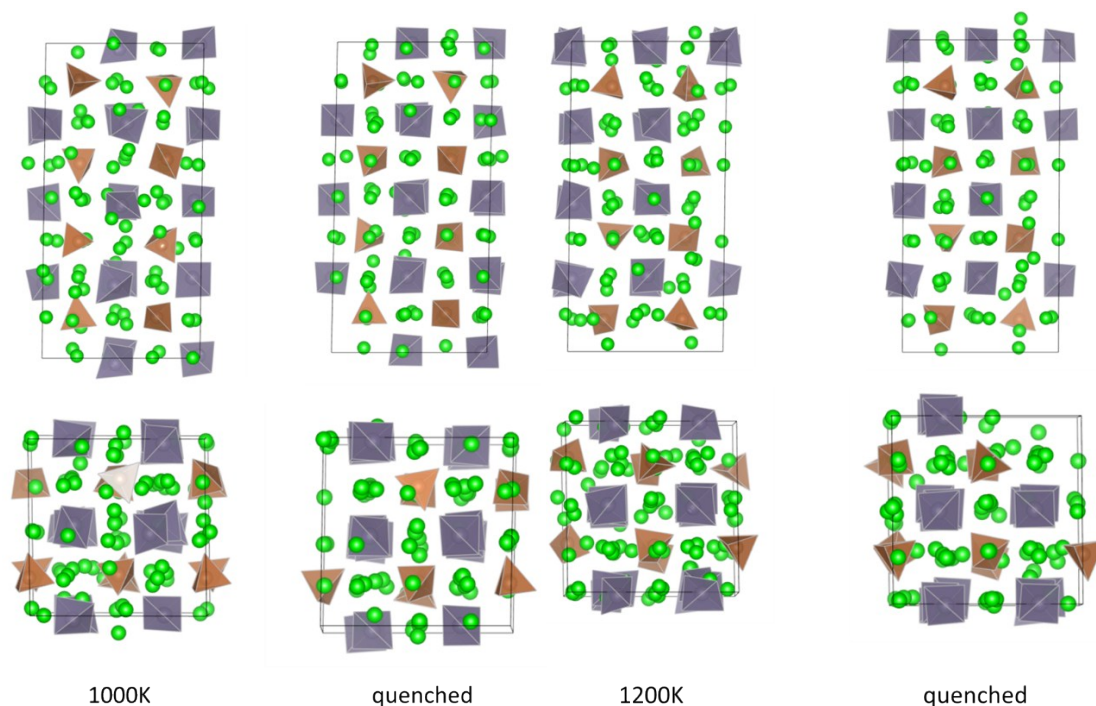
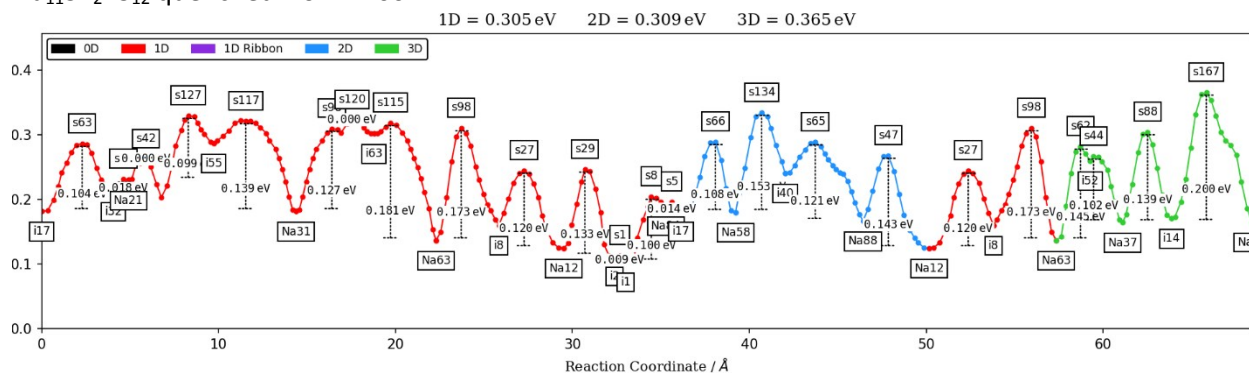
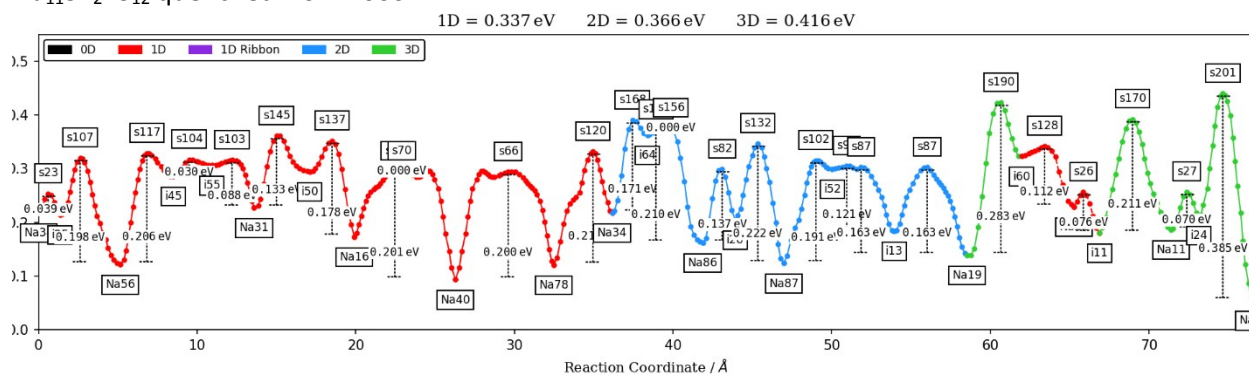
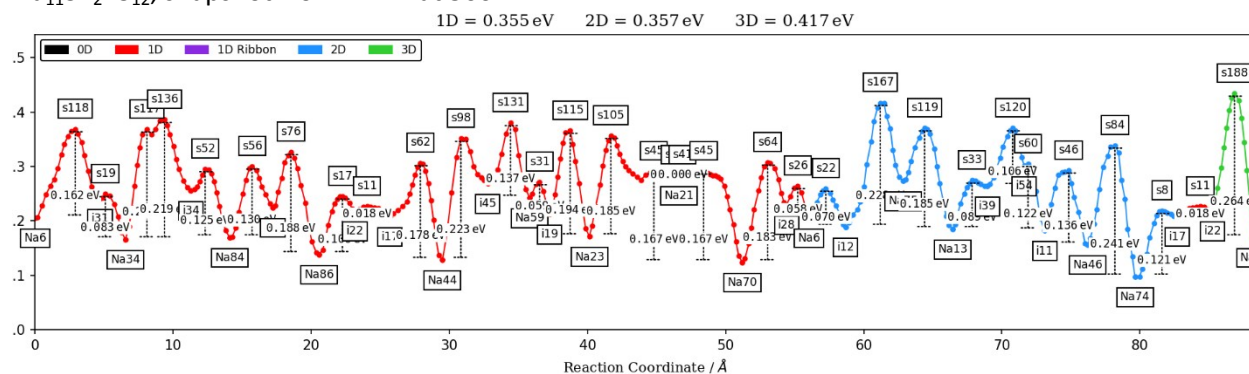
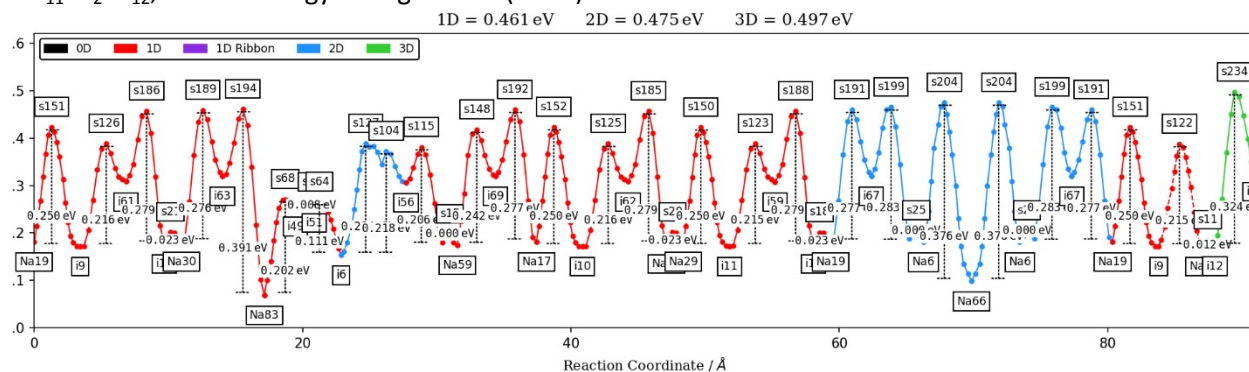
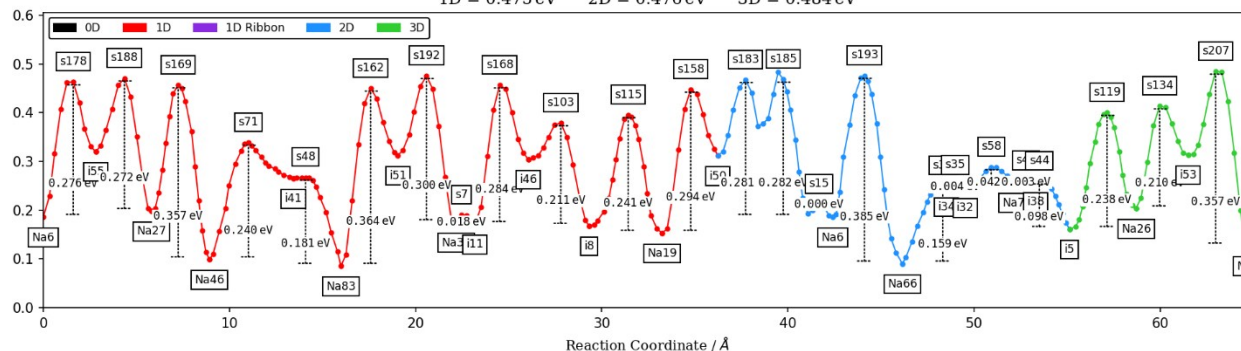


Figure S.6 Top and side views of Na₁₁Sn₂PS₁₂ at the end of the 80 ps NVT AIMD runs at T = 1000 K and T = 1200 K as well as of the relaxed structures derived from the above by geometry optimization (“quenching”). Na sites are marked as green spheres, SnS₄ (PS₄) as grey (brown) tetrahedra.

Na₁₁Sn₂PS₁₂ quenched from 1200 K:Na₁₁Sn₂PS₁₂ quenched from 1000 K:Na₁₁Sn₂PS₁₂, snapshot from AIMD at 500 KNa₁₁Sn₂PS₁₂, lowest energy configuration ("0 K"):

$\text{Na}_{11.25}\text{Sn}_{2.25}\text{P}_{0.75}\text{S}_{12}$, lowest energy configuration ("0 K"):

1D = 0.475 eV 2D = 0.476 eV 3D = 0.484 eV


 $\text{Na}_{10}\text{SnP}_2\text{S}_{12}$, lowest energy configuration ("0 K"):

1D = 0.378 eV 2D = 0.388 eV 3D = 0.459 eV

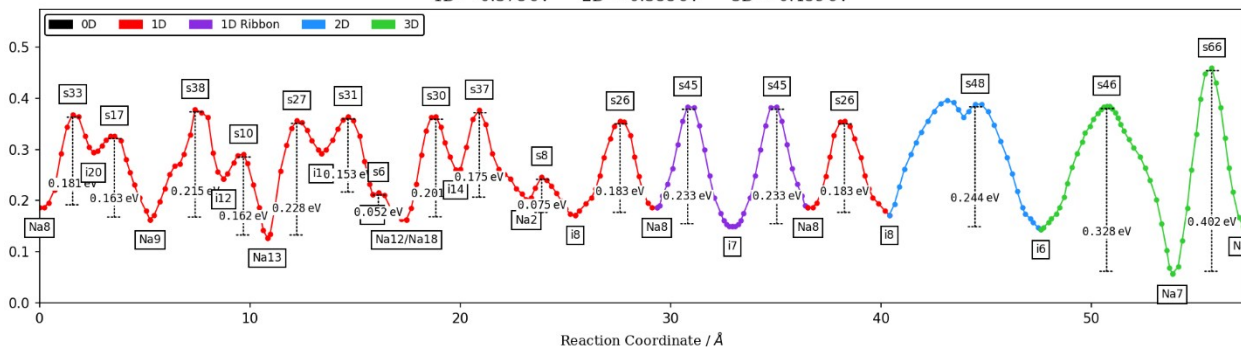


Figure S.7 Bond valence site energy models of barriers in energy landscapes for Na^+ migration in $\text{Na}_{11}\text{Sn}_2\text{PS}_{12}$ derived from the quenched structure models at $T = 1200$ K, 1000 K, an AIMD snapshot at $T = 500$ K, and various lowest energy configurations as well as average structures from literature X-ray diffraction studies. In all graphs the y-axis indicates the Na bond-valence site energy (BVSE) in eV relative to the BVSE minimum in the respective local structure model. The text line above each graph indicates the effective migration barriers for 1-, 2- or 3-dimensional percolation through the pathway network (in eV).

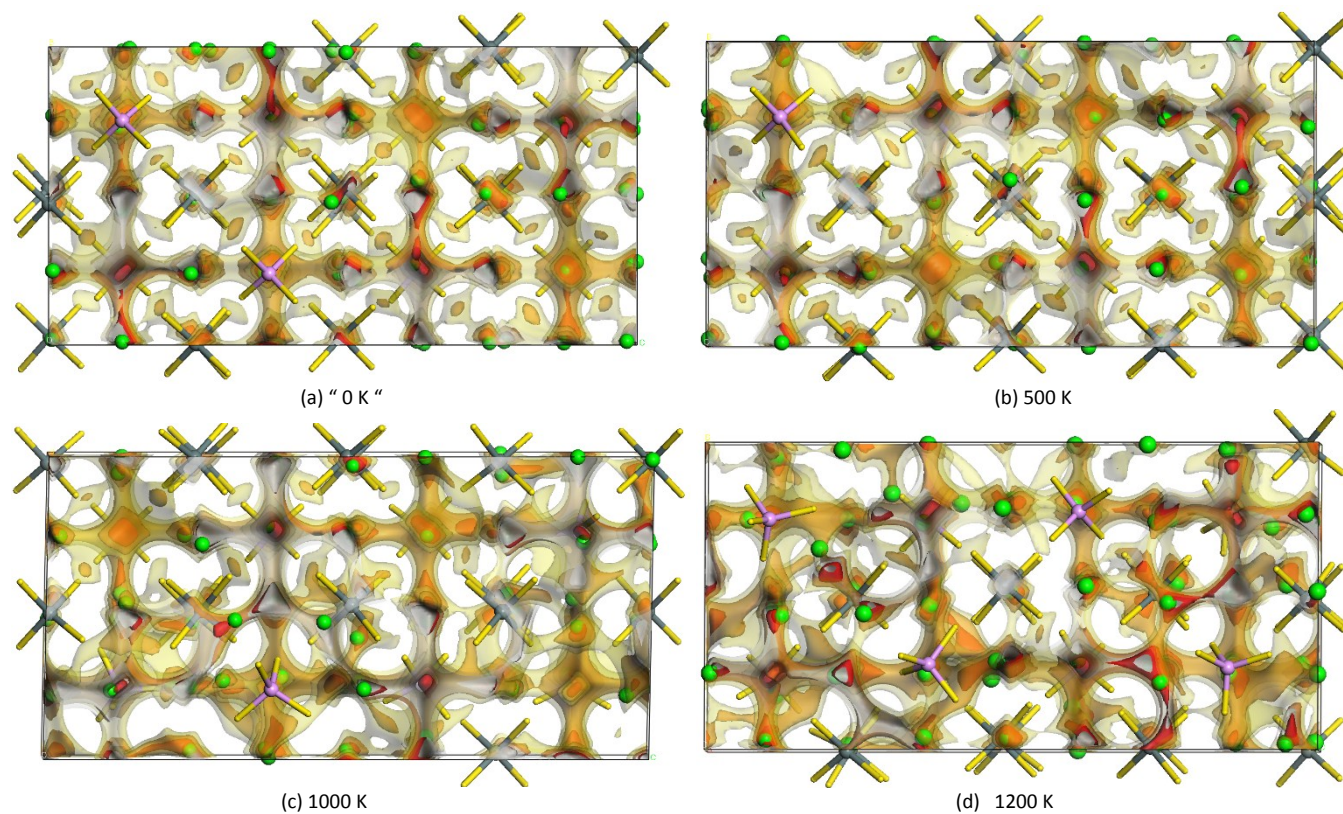


Figure S.8 Structure models superimposed on isosurfaces of constant bond valence site energy (BVSE) as a representation of the energy landscapes for Na⁺ migration in Na₁₁Sn₂PS₁₂ (a) the lowest energy configuration (“0 K”), or quenched from (b) T = 500 K, (c) T = 1000 K or (d) T = 1200 K and. In all graphs the same three isosurface values are chosen relative to the minimum BVSE(Na) in the respective structure model: 0.25 eV (red), 0.35 eV (orange) and 0.47 eV (yellow). Besides the pathways in the anion-ordered structures at T ≤ 500 K, the anion disorder in samples quenched from higher temperatures leads to a change in pathway topology.

5. Description of cif files supplied as Electronic Supplementary Information

1) The lowest energy structure of Na ₁₀ SnP ₂ S ₁₂ :	na10snp2s12.cif
2) The lowest energy structure of Na ₁₀ SnSb ₂ S ₁₂ :	na10snsb2s12.cif
3) The lowest energy structure of Na ₁₁ Sn ₂ PS ₁₂ :	na11sn2ps12_1.cif
4) The second lowest energy structure of Na ₁₁ Sn ₂ PS ₁₂ :	na11sn2ps12_2.cif
5) The lowest energy structure of Na ₁₁ Sn ₂ SbS ₁₂ :	na11sn2sbs12_1.cif
6) The structure of Na ₁₁ Sn ₂ PS ₁₂ , containing 7Na ₂ and 1Na ₃ vacancies:	na11sn2ps12_1na3.cif
7) The structure of Na ₁₁ Sn ₂ PS ₁₂ , containing 6Na ₂ and 2Na ₃ vacancies:	na11sn2ps12_2na3.cif
8) The structure of Na ₁₁ Sn ₂ PS ₁₂ , containing 5Na ₂ and 3Na ₃ vacancies:	na11sn2ps12_3na3.cif
9) The structure of Na ₁₁ Sn ₂ PS ₁₂ , containing 7Na ₂ and 1Na ₁ vacancies:	na11sn2ps12_na1.cif
10) The structure of Na ₁₁ Sn ₂ PS ₁₂ , containing 7Na ₂ and 1Na ₄ vacancies:	na11sn2ps12_na4.cif
11) The structure of Na ₁₁ Sn ₂ PS ₁₂ , containing 7Na ₂ and 1Na ₅ vacancies:	na11sn2ps12_na5.cif
12) The lowest energy structure of Na _{10.75} Sn _{1.75} P _{1.25} S ₁₂ (= Na ₈₆ Sn ₁₄ P ₁₀ S ₉₆):	na86sn14p10s96.cif
13) The lowest energy structure of Na _{10.75} Sn _{1.75} Sb _{1.25} S ₁₂ (= Na ₈₆ Sn ₁₄ Sb ₁₀ S ₉₆):	na86sn14sb10s96.cif
14) The lowest energy structure of Na _{10.875} Sn _{1.875} P _{1.125} S ₁₂ (= Na ₈₇ Sn ₁₅ P ₉ S ₉₆):	na87sn15p9s96.cif
15) The lowest energy structure of Na _{10.875} Sn _{1.875} Sb _{1.125} S ₁₂ (= Na ₈₇ Sn ₁₅ Sb ₉ S ₉₆):	na87sn15sb9s96.cif
16) The lowest energy structure of Na _{11.125} Sn _{2.125} P _{0.875} S ₁₂ (= Na ₈₉ Sn ₁₇ P ₇ S ₉₆):	na89sn17p7s96.cif
17) The lowest energy structure of Na _{11.125} Sn _{2.125} Sb _{0.875} S ₁₂ (= Na ₈₉ Sn ₁₇ Sb ₇ S ₉₆):	na89sn17sb7s96.cif
18) The lowest energy structure of Na _{11.25} Sn _{2.25} P _{0.75} S ₁₂ (= Na ₉₀ Sn ₁₈ P ₆ S ₉₆):	na90sn18p6s96.cif
19) The lowest energy structure of Na _{11.25} Sn _{2.25} Sb _{0.75} S ₁₂ (= Na ₉₀ Sn ₁₈ Sb ₆ S ₉₆):	na90sn18sb6s96.cif
20) The structure of Na ₁₁ Sn ₂ PS ₁₂ after 80ps of AIMD at 300K:	na11sn2ps12_300K.cif
21) The structure of Na ₁₁ Sn ₂ PS ₁₂ after 80ps of AIMD at 500K:	na11sn2ps12_500K.cif
22) The structure of Na ₁₁ Sn ₂ PS ₁₂ after 80ps of AIMD at 800K:	na11sn2ps12_800K.cif
23) The structure of Na ₁₁ Sn ₂ PS ₁₂ after 80ps of AIMD at 1000 K and relaxation	na11sn2ps12_1000K-quenched.cif

References

- G. Kresse, J. Furthmüller, *Phys. Rev. B*, 1996, **54**, 11169.
- G. Kresse, J. Furthmüller, *Comput. Mater. Sci.*, 1996, **6**, 15–50.
- P. E. Blöchl, *Phys. Rev. B*, 1994, **50**, 17953.
- J. P. Perdew, K. Burke, M. Ernzerhof, *Phys. Rev. Lett.*, 1996, **77**, 3865–3868.
- J. P. Perdew, A. Ruzsinszky, G. I. Csonka, O. A. Vydrov, G. A. Scuseria, L. A. Constantin, X. Zhou, K. Burke, *Phys. Rev. Lett.*, 2008, **100**, 136406.
- P. E. Blöchl, O. Jepsen, O. K. Andersen, *Phys. Rev. B*, 1994, **49**, 16223.
- K. Momma, F. Izumi, *J. Appl. Crystallogr.*, 2011, **44**, 1272–1276.
- S. Nose, *J. Chem. Phys.*, 1984, **81**, 511–519.
- W. G. Hoover, *Phys. Rev. A: At., Mol., Opt. Phys.*, 1985, **31**, 1695–1697.
- L. Verlet, *Phys. Rev.*, 1967, **159**, 98–103.
- R. Prasada Rao, H. Chen, S. Adams, *Chem. Mater.*, 2019, **31**, 8649–8662.
- H. Chen, L. L. Wong, S. Adams, *Acta Crystallogr. B*, 2019, **75**, 18–33.
- S. Adams, “Practical Considerations in Determining Bond Valence Parameters”, in “Bond Valences” (Brown, I.D.; Poeppelmeier, K.R.; eds.), Springer Berlin Heidelberg, Structure and Bonding 2014, **158**, 91–128. (doi:10.1007/430_2013_96).
- S. Adams, R. Prasada Rao, *Solid State Ionics*, 2011, **184**, 57–61.
- H. Chen, S. Adams, *IUCrJ*, 2017, **4**, 614–625.
- Z. Yu, S.-L. Shang, Y. Gao, D. Wang, X. Li, Z.-K. Liu, D. Wang, *Nano Energy*, 2018, **47**, 325–330.
- J. W. Heo, A. Banerjee, K. H. Park, Y. S. Jung, S.-T. Hong, *Adv. Energy Mat.*, 2018, **1**, 1702716.
- L. Liu, Z. Lu, M. B. Effata, F. Ciuccia, *J. Power Sources*, 2019, **409**, 94–101.
- Z. Zhang, E. Ramos, F. Lalère, A. Assoud, K. Kaup, P. Hartman, L. F. Nazar, *Energy Environ. Sci.*, 2018, **11**, 87–93.
- M. Duchardt, U. Ruschewitz, S. Adams, S. Dehnen, B. Roling, *Angew. Chem. Int. Ed.*, 2018, **57**, 1351–1355.
- K. Oh, D. Chang, I. Park, K. Yoon, K. Kang, *Chem. Mater.*, 2018, **31**, 6066–6075.
- E. P. Ramos, Z. Zhang, A. Assoud, K. Kaup, F. Lalère, L. F. Nazar, *Chem. Mat.* 2018, **30**, 7413–7417.
- W. D. Richards, T. Tsujimura, L. J. Miara, Y. Wang, J. C. Kim, S. P. Ong, I. Uechi, N. Suzuki, G. Ceder, *Nat. Commun.*, 2016, **7**, 11009.